An Adaptive-Gain Complementary Filter for Real-Time Human Motion Tracking With MARG Sensors in Free-Living Environments

Ya Tian, *Student Member, IEEE*, Hongxing Wei, *Member, IEEE*, and Jindong Tan, *Member, IEEE*

***Abstract*—High-resolution, real-time data obtained by human motion tracking systems can be used for gait analysis, which helps better understanding the cause of many diseases for more effective treatments, such as rehabilitation for outpatients or recovery from lost motor functions after a stroke. In order to achieve real-time ambulatory human motion tracking with low-cost MARG (magnetic, angular rate, and gravity) sensors, a computationally efficient and robust algorithm for orientation estimation is critical. This paper presents an analytically derived method for an adaptive-gain complementary filter based on the convergence rate from the Gauss–Newton optimization algorithm (GNA) and the divergence rate from the gyroscope, which is referred as adaptive-gain orientation filter (AGOF) in this paper. The AGOF has the advantages of one iteration calculation to reduce the computing load and accurate estimation of gyroscope measurement error. Moreover, for handling magnetic distortions especially in indoor environments and movements with excessive acceleration, adaptive measurement vectors and a reference vector for earth's magnetic field selection schemes are introduced to help the GNA find more accurate direction of gyroscope error. The features of this approach include the accurate estimation of the gyroscope bias to correct the instantaneous gyroscope measurements and robust estimation in conditions of fast motions and magnetic distortions. Experimental results are presented to verify the performance of the proposed method, which shows better accuracy of orientation estimation than several well-known methods.**

***Index Terms*—Adaptive-gain complementary filter, Gauss–Newton optimization algorithm (GNA), human motion capture (MoCap), magnetic, angular rate and gravity (MARG) sensors, quaternion-based orientation.**

I. Introduction

RECENTLY, the development of human motion capture system (MoCap, or motion tracking) [1] has been highly stimulated by clinical medicine, where gait analysis is the major application of motion capture. High-resolution, quantitative data obtained by these systems can be used to better understand the cause of many diseases for more effective treatments. Examples include rehabilitation for outpatients or those people who have suffered a stroke to recover the lost motor function [2], fall characteristics [3], activity level [4], functional behavior following arthroplasties [5], [6], and biomechanical loading of joints [7]. Continuous monitoring of human movement in the patient's natural living environment potentially provides more valuable feedback to guide clinical interventions. However, it has been extremely challenging to go beyond laboratory environments and obtain accurate measurements of human physical activity especially in free-living environments. Commercial motion-capture systems produce excellent in-studio capture and reconstructions, but need an external source (e.g., cameras) and offer no comparable solution for acquiring information from patients in everyday environments.

Recent developments in miniature sensor technology have led many researchers to utilize wearable inertial sensors to capture human movement out of controlled volumes. The popularity of these wearable sensors for human motion capture mainly comes from the fact that they are independent from an infrastructure and do not require an external source. In addition, these sensors are relatively low cost, light weight and compact in size due to the advances in miniature sensor technology, so they have the potential to measure limb movements, posture, and other physiological conditions in human's free-living environments for the practice of physical medicine and rehabilitation. Meanwhile, with the advances in wireless sensor networks, these sensors apply different networking technologies such as Bluetooth and IEEE 802.15.4, which make the attachment of sensors much easier. Therefore, the "wearable" sensing mainly means that miniature sensors can be unobtrusively attached to the human body, thus opening the possibility of human daily activities monitoring in free-living environments.

Usually, a human body can be modeled as a multi-link system comprising several body segments connected by joints, which is referred as a kinematic chain. If the orientation relative to each segment can be determined, then the overall motion of the human body can be calculated based on this kinematic chain. Therefore, the accurate estimation of human joint angle plays an important role in human motion analysis [8]. The orientation of individual limb segments can be measured through the attachment of an inertial/magnetic sensor module. Such a sensor module typically consists of a tri-axis accelerometer, a tri-axis gyroscope, and a tri-axis magnetometer and is compact in size, which can be called wearable MARG (magnetic, angular rate and gravity) sensor [9].

Manuscript received October 13, 2011; revised March 23, 2012; accepted June 15, 2012. Date of publication July 12, 2012; date of current version March 07, 2013.

Y. Tian is with the School of Information and Electrical Engineering, Shandong Jianzhu University, Jinan, Shandong 250101, China, and also with the Department of Electrical and Computer Engineering, Michigan Technological University, Houghton, MI 49931 USA (e-mail: tya@mtu.edu).

H. Wei is with the School of Mechanical Engineering and Automation, Beihang University, Beijing 100191, China, and also with the Electrical Engineering Department, Michigan Technological University, Houghton, MI 49931 USA. (e-mail: weihongxing@buaa.edu.cn).

J. Tan is with the Department of Mechanical, Aerospace and Biomedical Engineering, The University of Tennessee, Knoxville, TN 37996 USA. (e-mail: tan@utk.edu).

Digital Object Identifier 10.1109/TNSRE.2012.2205706

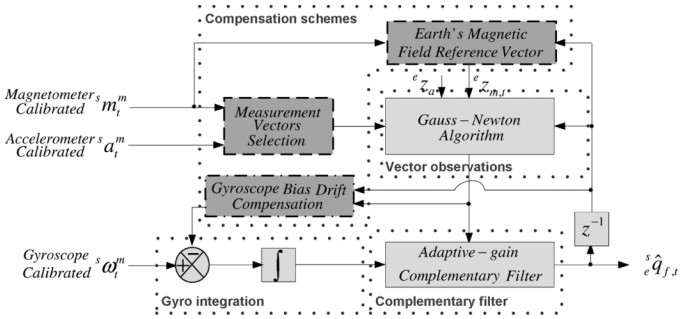

Fig. 1. Main framework of the proposed method (AGOF) for orientation estimation.

However, there are two major challenges for estimating orientation using a MARG sensor. First, directly integrating the angular velocity from the tri-axis gyroscope provides a challenge, because the orientation estimation accuracy is negatively affected by physical limitations inherent in inertial sensors, which manifest as noise present in the output of these sensors and quickly cause drift accumulation in a long-term tracking [10]. The accumulated drift during a long-term tracking prevents its effective application in human motion capture for quantitative assessment. Secondly, as aiding sensors for mitigating the drift in orientation, the tri-axis accelerometers and magnetometers are employed for the vertical (earth's gravity) and the horizontal (earth's magnetic field) references, respectively. However, accelerometers are sensitive to body accelerations (besides gravity) under dynamic motion conditions, while magnetometer measurements suffer from local earth magnetic field variations, which are easily caused by common everyday objects, such as operating electrical appliances or objects made of ferrous materials [11]. These variations influence the direction of the earth's magnetic field, further affecting the desired orientation estimation. Furthermore, both outputs contain measurement errors as well.

In order to overcome these challenges, an adaptive-gain orientation filter (AGOF) is proposed in this paper based on the basic theory of deterministic approach and frequency-based approach, and it is tested on a newly developed MARG sensor. The main framework of the proposed AGOF includes four major parts: 1) gyro integration; 2) vector observations; 3) complementary filter; and 4) compensation schemes, which are shown as dotted blocks in Fig. 1. One main feature of the proposed work is the development of an analytically derived method for the adaptive-gain complementary filter based on the convergence rate from the GNA and the divergence rate from the gyroscope, which has the advantages of not only one iteration calculation to reduce the computing load but also accurate direction of the gyroscope measurement error. As a result, a real-time orientation tracking can be achieved due to inexpensive computation, and the gyroscope bias drift can be compensated for through the integral feedback of the error in the rate of change of orientation, shown as the dashed–dotted block in "Compensation schemes" of Fig. 1. Moreover, when severe magnetic distortions (especially for indoor estimation) or highly dynamic movements with extra acceleration (besides gravity) happen, two more compensation schemes are developed for more efficient performance, which are adaptive measurement vectors selection and a reference vector for earth's magnetic field selection in combination with the GNA, also shown as dashed blocks in "Compensation schemes" of Fig. 1.

The main contributions of this paper are summarized as follows: 1) an analytical approach of combining the GNA with a complementary filter for faster quaternion updates; 2) adaptive measurement vectors and a reference vector for earth's magnetic field selection schemes in conjunction with the GNA; 3) a gyroscope bias drift compensation scheme for one input of the complementary filter; and 4) an adaptive-gain complementary filter based on the convergence rate from the GNA and the divergence rate from the gyroscope. Using the proposed algorithm, a real-time, drift-free, and accurate orientation tracking can be achieved even in the situation of temporary severe magnetic distortions and dynamic movements. The accuracy of the proposed algorithm is experimentally validated using the newly developed MARG measurements, compared with the results from the Vicon system [12] and three other well-known algorithms including Kalman-based filter (KF), factored quaternion algorithm (FQA) proposed in [13], and gradient descent algorithm (GDA) proposed in [14].

II. Related Work

Recently, the benefits of MARG sensors have attracted more and more researchers to develop advanced and novel algorithms to alleviate accumulated drifts. These algorithms are usually based on three major approaches to mitigate the sensing errors: 1) stochastic approach (Kalman filter); 2) deterministic approach (the Wahba's problem); and 3) frequency-based approach (complementary filter). In this section, related work on these three approaches is introduced.

A. The Stochastic Approach

Kalman filter is one of the most often used stochastic approaches to account for the noise statistics. In [15] and [16], Luinge *et al.* used an inclination estimate from an accelerometer to reduce the integration drift originated from a gyroscope and a Kalman filter for taking into account the fluctuating gyroscope offset. Tatsuya *et al.* [17] developed a portable orientation estimating device equipped with a gyroscope, accelerometer, and magnetometer. The accelerometer and magnetometer were used to measure the absolute orientation against the earth and the gyroscope was used to measure the local angular velocity. An unscented Kalman filter (UKF) was used to fuse these three sensors in this paper. Similarly, a quaternion-based extended Kalman filter (EKF) [18] was developed for determining the orientation of a rigid body. In [19], Roetenberg *et al.* proposed a complementary Kalman filter to estimate orientation of human body segments. In the filter, the gyroscope bias error, orientation error, and magnetic disturbance error were estimated.

However, the Kalman filter implementation would impose an unacceptable computational burden due to so many recursive formulas which need to be calculated to make the mean squared error least [20]. Furthermore, different kinds of Kalman filters are needed for different state vectors, dynamic models and measurement models; and with the increase of accuracy of the result, the larger dimension state vectors are needed, which will lead to higher computation costs.

B. The Deterministic Approach

The deterministic approaches are originated from the "Wahba's problem" [21]–a variation of the least square minimization problems. It is used to find a best fit orientation estimation solution from redundant sensor measurements. One of the solutions to this problem is the well-known QUEST (QUaternion ESTimator) algorithm [22] usually used in multi-dimension vector optimization, such as the gradient descent algorithm (GDA) and the Gauss–Newton algorithm (GNA). With two vector measurements that can be used for calculating the absolute orientation against the earth, an optimization method can achieve the goal. However, an optimization method usually needs multiple iterations and matrix inverse computation, even though a reduced order GNA was proposed in [9] and [23]. Yun *et al.* [13] also proposed an algorithm for an orientation estimation from earth gravity and magnetic field measurements without using QUEST or optimization method. This innovative method significantly reduced computation requirements towards real time computation on resource constrained hardware. However, this method can only be restricted to a static or slow movement without magnetic field variations. Similarly, the solutions based on Wahba's problem have the same disadvantage as the method presented in [13], which was only applied to static or low-frequency situations. In this paper, the proposed AFOF tries to handle these issues using three strategies, one of which is the adaptive measurement vectors selection. The AGOF uses the second strategy of an adaptive reference vector of the earth's magnetic field to get better yaw angle estimation than those proposed in [14] and [23]. A gyroscope bias drift compensation is the third strategy utilized for more efficient performance in case of no need for vector designation happened [23] and the orientation estimation totally relied on the gyro output.

C. The Frequency-Based Approach

The idea behind the frequency-based approach, mainly in the form of a complementary filter [24]–[26], is to pass one signal through a low-pass filter and the other one through a high-pass filter and combine them to give the final rate. Therefore, it can be better to combine slow moving signals from the accelerometer and magnetometer, and fast moving signals from the gyroscope. An adaptive-gain complementary filter is designed in this paper as opposed to the convention complementary filter. Even though the authors in [26] proposed an adaptive-gain complementary filter for orientation estimation, the optimal value of filter gain in this paper is more robust, because the gain of the proposed filter is adaptively adjusted by using the convergence rate of orientation estimation from vector observations based on the GNA and the divergence rate of orientation estimation from the gyroscope without choosing any threshold, which is usually obtained by numerical experiments and may not be robust for every trail.

III. Problem Formulation

This section outlines a quaternion representation of orientation for the sensor arrays, modeling of the sensors, and sensor calibration to formulate the orientation estimation problem. For clarity, the definitions of mathematical variables are firstly described as follows.

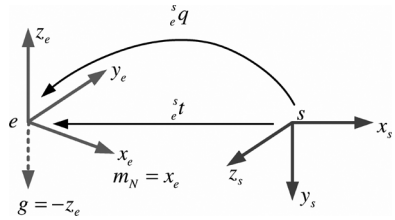

Fig. 2. Relation between the earth frame (e) and sensor frame (s) and the respective transformation based on unit quaternion.

- s: Indicating the sensor frame affiliated to the sensor.
- e: Indicating the earth frame.
- $\boldsymbol{g}$: Gravity vector.
- ${}^s\boldsymbol{a}$: Measurements from accelerometer in the sensor frame.
- ${}^s\boldsymbol{\omega}$: Measurements from gyroscope in the sensor frame.
- ${}^s\boldsymbol{m}$: Measurements from magnetometer in the sensor frame.
- ${}^s_e\boldsymbol{q}_t$: Quaternion-based orientation from sensor frame to earth frame at time t.
- ${}^s_e\hat{\boldsymbol{q}}_{\omega,t}$: Orientation estimated from gyroscope at time t.
- ${}^s_e\hat{\boldsymbol{q}}_{a,t}$: Orientation estimated from accelerometer and magnetometer at time t.
- ${}^s_e\hat{\boldsymbol{q}}_{f,t}$: Orientation estimated from complementary filter fusion at time t.

A. Quaternion Representation

The orientation of a rigid body in space is determined when the axes orientation of a coordinate frame (the sensor frame s) attached to the body are specified with respect to an absolute coordinate system, usually named the earth frame e (x_e axis pointing to local magnetic north and the z_e axis pointing opposite gravity), as shown in Fig. 2. In order to easily represent the rotation between these two coordinate frames, it is important to have a good mathematical representation. There are three mathematical rotational representations in common usage: Euler angles, rotation matrix, and quaternion. In this paper, quaternion-based rotation ${}^s_e\boldsymbol{q}$ is used, because Euler angles suffer from singularities in despite of less parameters and rotation matrix has more parameters with less computational efficiency.

A quaternion can be thought of as a vector with four components, as a composite of a scalar s and an ordinary vector $\boldsymbol{u}$. A rotation about an unit vector $\boldsymbol{v} = [v_x, v_y, v_z]$ by an angle θ can be computed using quaternion shown in (1). If this unit vector $\boldsymbol{v}$ is defined in frame s, frame e can be achieved by rotating frame s the angle θ around this unit vector $\boldsymbol{v}$, so the relative orientation between s and e can be represented by the unit quaternion ${}^s_e\boldsymbol{q}$ in (2), which denotes the orientation of frame s relative to frame e [27]

$$\boldsymbol{q} = (s, \boldsymbol{u}) = \left(\cos\frac{\theta}{2} \;\; \boldsymbol{v}\sin\frac{\theta}{2}\right) \tag{1}$$

$$\begin{aligned} {}^s_e\boldsymbol{q} &= [q_0 \; q_x \; q_y \; q_z] \\ &= \left[\cos\frac{\theta}{2} \quad v_x\sin\frac{\theta}{2} \quad v_y\sin\frac{\theta}{2} \quad v_z\sin\frac{\theta}{2}\right]. \end{aligned} \tag{2}$$

As we mentioned above, frame e can be obtained through a rotation of angle θ around an unit vector ${}^s\boldsymbol{v}$ (the super-script s indicates this vector defined in frame s) and the orientation of frame s relative to frame e can be denoted by an unit quaternion

${}^s_e\boldsymbol{q}$. So this unit vector defined in frame e, ${}^e\boldsymbol{v}$, can be calculated using the relationship described in

$$ {}^e\boldsymbol{v} = {}^s_e\boldsymbol{q} \otimes {}^s\boldsymbol{v} \otimes {}^s_e\boldsymbol{q}^* \tag{3}$$

where $\otimes$ denotes the quaternion product [28]. ${}^s_e\boldsymbol{q}^*$ denotes the conjugate of ${}^s_e\boldsymbol{q}$ and actually equals to ${}^e_s\boldsymbol{q}$, defined as

$$ {}^s_e\boldsymbol{q}^* = {}^e_s\,\boldsymbol{q} = [q_0 \; -q_x \; -q_y \; -q_z]. \tag{4}$$

B. Sensor Modeling

Based on the limitation of the MARG sensor, and the fact that the proposed algorithm is implemented on the newly developed low-cost chip, the measurement models for the gyroscope, accelerometer, and magnetometer are briefly discussed in following sections.

1) Gyroscope: The measured gyroscope signal ${}^s\boldsymbol{\omega}^m_t$ can be represented in the sensor frame s at time t using

$$ {}^s\boldsymbol{\omega}^m_t = {}^s\boldsymbol{\omega}_t + \boldsymbol{b}_{\omega,t} + \boldsymbol{e}_{\omega,t} \tag{5}$$

where ${}^s\boldsymbol{\omega}_t$ is the ture angular velocity after compensation. $\boldsymbol{b}_{\omega,t}$ is the bias which is caused by low-frequency offset fluctuations. Actually, it determines the worst case drift when integrating the gyroscope signal. The remaining error $\boldsymbol{e}_{\omega,t}$ is assumed to be the zero-mean white noise.

2) Accelerometer: Similar to the gyroscope signal, the measured accelerometer signal ${}^s\boldsymbol{a}^m_t$ can be represented using

$$\begin{aligned} {}^s\boldsymbol{a}^m_t &= {}^s\boldsymbol{a}_t + \boldsymbol{b}_{a,t} + \boldsymbol{e}_{a,t} \\ {}^s\boldsymbol{a}_t &= {}^s\boldsymbol{a}_{b,t} + {}^s\boldsymbol{g}_t \end{aligned} \tag{6}$$

where ${}^s\boldsymbol{a}_t$ is the linear acceleration after error compensation. ${}^s\boldsymbol{a}_{b,t}$ is the body linear acceleration after gravity compensation. $\boldsymbol{b}_{a,t}$ is the bias which is caused by low-frequency offset. Actually, it determines the worst case drift when double integrating the accelerometer signal. The remaining error $\boldsymbol{e}_{a,t}$ is assumed to be the zero-mean white noise. In the earth frame e, gravity is a constant vector representing the vertical direction. However, if it is expressed in sensor frame s, it depends on the orientation of the MARG sensor. This means that the inclinational direction can be estimated when the free acceleration is known, or alternatively, the free acceleration can be calculated from the accelerometer signal, when the orientation is known.

3) Magnetometer: For the magnetometer, the measured signal ${}^s\boldsymbol{m}^m_t$ is often modeled as the sum of the earth's magnetic field ${}^s\boldsymbol{m}_t$, magnetic disturbance $\boldsymbol{d}_{m,t}$, magnetic bias $\boldsymbol{b}_{m,t}$ and noise $\boldsymbol{e}_{m,t}$, as shown in

$$ {}^s\boldsymbol{m}^m_t = {}^s\,\boldsymbol{m}_t + \boldsymbol{d}_{m,t} + \boldsymbol{b}_{m,t} + \boldsymbol{e}_{m,t}. \tag{7}$$

C. Sensor Calibration

Since the accuracy of the orientation estimate depends heavily on the MARG measurements and the bias error is the major factor of accumulated drift for long-time tracking, it is imperative to remove the bias error of each sensor least. So in this paper, the *null point* and *scale factor* of each axis of the MARG sensor are determined using the method described in [29]. Moreover, calibration procedure should be taken before each practical use, unless the characteristics of the sensors themselves change little. For the newly developed low-cost MARG sensor, sensor calibration is needed before each experimental trial. After bias error compensation for each sensor, the outputs of the MARG sensor represented in (5)–(7) can be rewritten as ${}^s\boldsymbol{\omega}^m_t \approx {}^s\boldsymbol{\omega}_t + \boldsymbol{e}_{\omega,t}$, ${}^s\boldsymbol{a}^m_t \approx {}^s\boldsymbol{a}_{b,t} + {}^s\boldsymbol{g}_t + \boldsymbol{e}_{a,t}$, and ${}^s\boldsymbol{m}^m_t \approx {}^s\boldsymbol{m}_t + \boldsymbol{d}_{m,t} + \boldsymbol{e}_{m,t}$, which are used as inputs of the proposed algorithm. Particularly, the proposed algorithm itself can be good at handling the zero-mean white noise.

After finishing modeling and calibrating the sensor measurements from the newly developed MARG, all measurements are represented in the form of quaternions as inputs of the proposed algorithm. In order to mitigate the accumulated drift from directly integrating the linear angular velocity of the gyroscope, the accelerometer and magnetometer are used as aiding sensors for providing the vertical and horizontal references of earth. In this paper, the GNA is chosen to process vector observations due to its faster convergent rate. An analytically derived method is developed based on the combination theory of the GNA and a simple complementary filter, where only one iteration is performed to reduce the computing load. It is also an important step for real-time tracking. In addition, the gain of the complementary filter is adaptively adjusted based on the convergence rate from the GNA and the divergence rate from the gyroscope. Moreover, considering the challenges from aiding sensors, which are subject to severe magnetic distortions and highly dynamic movements, three strategies are developed to handle them, which are the adaptive measurement vectors selection, adaptive reference vector of earth's magnetic field, and gyroscope bias drift compensation scheme. Finally, a real-time, drift-free, and accurate quaternion-based orientation ${}^s_e\hat{\boldsymbol{q}}_{f,t}$ can be obtained. The next section will detail the proposed method—adaptive-gain orientation filter.

IV. Adaptive-Gain Orientation Filter

In this section, an adaptive-gain orientation filter (AGOF) is designed to find the best fit by fusing fast moving signals from the gyroscope and slow moving signals from vector observations based on the GNA. Four major components of the proposed filter shown in Fig. 1 are described in details. Furthermore, an extra section called "Filter Gains" is presented to discuss the determination of the filter gains.

A. Orientation Estimation From Gyroscope

The tri-axis gyroscope measures the angular velocities ${}^s\boldsymbol{\omega}$ which is expressed in the sensor frame s. For convenience, this ${}^s\boldsymbol{\omega}$ is represented as a four-element row vector: ${}^s\boldsymbol{\omega} = [0 \; \omega_x \; \omega_y \; \omega_z]$ using the quaternion representation. The quaternion derivation ${}^s_e\dot{\boldsymbol{q}}$ describing the rate of change of orientation in the sensor frame relative to the earth frame can be calculated as

$$ {}^s_e\dot{\boldsymbol{q}} = \frac{1}{2}{}^s_e\hat{\boldsymbol{q}} \otimes {}^s\boldsymbol{\omega} = \frac{1}{2}\boldsymbol{\Omega}({}^s\boldsymbol{\omega}){}^s_e\hat{\boldsymbol{q}} \tag{8}$$

where $\boldsymbol{\Omega}({}^s\boldsymbol{\omega})$ is the 4×4 skew-symetric matrix of a quaternion ${}^s\boldsymbol{\omega} = [0 \; \omega_x \; \omega_y \; \omega_z]$, which can be represented as:

$$ \boldsymbol{\Omega}({}^s\boldsymbol{\omega}) = \begin{bmatrix} 0 & -\omega_x & -\omega_y & -\omega_z \\ \omega_x & 0 & \omega_z & -\omega_y \\ \omega_y & -\omega_z & 0 & \omega_x \\ \omega_z & \omega_y & -\omega_x & 0 \end{bmatrix}. \tag{9}$$

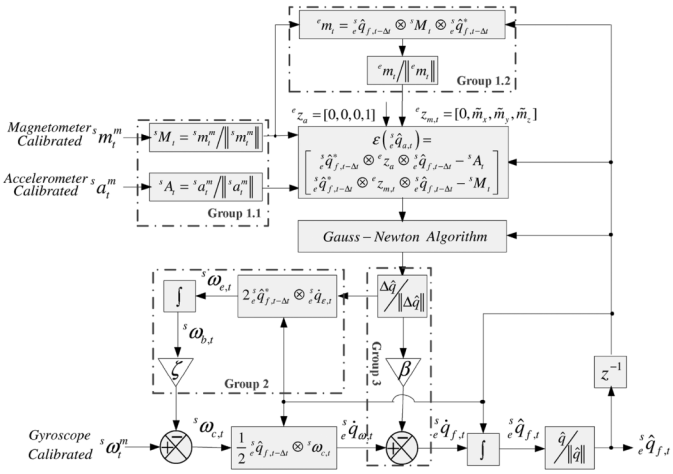

Fig. 3. Block diagram of the proposed adaptive-gain orientation filter design for MARG sensor arrays.

Therefore, the orientation of the sensor frame relative to the earth frame at time $t+\Delta t$, ${}^{s}_{e}\boldsymbol{q}_{\omega,t+\Delta t}$, can be calculated by integrating the quaternion time derivation ${}^{s}_{e}\dot{\boldsymbol{q}}_{\omega,t+\Delta t}$ as described by (10) with known initial condition ${}^{s}_{e}\hat{\boldsymbol{q}}_{\omega,t}$. Here, the subscript ω denotes that the orientation based on quaternion representation is obtained from the gyroscope readings

$$\begin{aligned} {}^{s}_{e}\dot{\boldsymbol{q}}_{\omega,t+\Delta t} &= \frac{1}{2}{}^{s}_{e}\hat{\boldsymbol{q}}_{\omega,t} \otimes {}^{s}\boldsymbol{\omega}_{t+\Delta t} \\ {}^{s}_{e}\boldsymbol{q}_{\omega,t+\Delta t} &= {}^{s}_{e}\hat{\boldsymbol{q}}_{\omega,t} + {}^{s}_{e}\dot{\boldsymbol{q}}_{\omega,t+\Delta t}\Delta t \end{aligned} \tag{10}$$

where Δt is the sampling time and ${}^{s}_{e}\hat{\boldsymbol{q}}_{\omega,t}$ is the previous orientation estimation represented by unit quaternion, which can also be obtained by using iterative equations (10).

B. Fast Gauss–Newton Method for Vector Observations

1) Problem Description: Since the accelerometer and magnetometer can measure the absolute orientation against the earth, the orientation from their measurements could be computed using a fast convergence approach called the Gauss–Newton optimization method. Given their normalized reference directions in the earth frame (${}^{e}\boldsymbol{z}_{a} = [0\ 0\ 0\ 1]$ for the accelerometer and ${}^{e}\boldsymbol{z}_{m,t} = [0\ \tilde{m}_x\ \tilde{m}_y\ \tilde{m}_z]$ for the magnetometer, which will be initially equal to ${}^{s}\boldsymbol{m}_{t=0}/\|{}^{s}\boldsymbol{m}_{t=0}\|$ and adaptively changed based on the current magnetometer measurements and the previous estimated orientation, shown as Group 1.2 in Fig. 3, when the magnetic distortion happens [see Section IV-D2]) and their normalized measurements shown in (11), the problem for finding the unit quaternion ${}^{s}_{e}\hat{\boldsymbol{q}}_{t}$ based on

$$\begin{aligned} {}^{s}\boldsymbol{A}_t &= \frac{{}^{s}\boldsymbol{a}^{m}_{t}}{\|{}^{s}\boldsymbol{a}^{m}_{t}\|} = [0\ a_{x,t}\ a_{y,t}\ a_{z,t}] \\ {}^{s}\boldsymbol{M}_t &= \frac{{}^{s}\boldsymbol{m}^{m}_{t}}{\|{}^{s}\boldsymbol{m}^{m}_{t}\|} = [0\ m_{x,t}\ m_{y,t}\ m_{z,t}] \end{aligned} \tag{11}$$

the Gauss–Newton method can be modeled as follows:

$$\begin{aligned} \text{find}: {}^{s}_{e}\hat{\boldsymbol{q}}_t &= [\hat{q}_0\ \hat{q}_x\ \hat{q}_y\ \hat{q}_z] \\ \text{minimize}: \boldsymbol{f}({}^{s}_{e}\hat{\boldsymbol{q}}_t) &= \frac{1}{2}\boldsymbol{\epsilon}({}^{s}_{e}\hat{\boldsymbol{q}}_t)^T\boldsymbol{\epsilon}({}^{s}_{e}\hat{\boldsymbol{q}}_t) \\ \text{where}: \boldsymbol{\epsilon} &= \begin{cases} \boldsymbol{\epsilon}_a({}^{s}_{e}\hat{\boldsymbol{q}}_t) = {}^{s}_{e}\hat{\boldsymbol{q}}_t \otimes {}^{e}\boldsymbol{z}_a \otimes {}^{s}_{e}\hat{\boldsymbol{q}}^{*}_t - {}^{s}\boldsymbol{A}_t \\ \boldsymbol{\epsilon}_m({}^{s}_{e}\hat{\boldsymbol{q}}_t) = {}^{s}_{e}\hat{\boldsymbol{q}}_t \otimes {}^{e}\boldsymbol{z}_{m,t} \otimes {}^{s}_{e}\hat{\boldsymbol{q}}^{*}_t - {}^{s}\boldsymbol{M}_t \end{cases} \\ \text{subject to}: {}^{s}_{e}\hat{\boldsymbol{q}}_t &\in \mathbb{R}^4 \ \text{and}\ {}^{s}_{e}\hat{\boldsymbol{q}}_t{}^{s}_{e}\hat{\boldsymbol{q}}^{T}_t = \|{}^{s}_{e}\hat{\boldsymbol{q}}_t\|^2 = 1 \end{aligned}$$

where $\boldsymbol{f}$ is the cost function, defined as the square of the error function $\boldsymbol{\epsilon} = [\boldsymbol{\epsilon}_a\ \ \boldsymbol{\epsilon}_m]^T$ which combines $\boldsymbol{\epsilon}_a$ from the accelerometer and $\boldsymbol{\epsilon}_m$ from the magnetometer together. It can be represented by using the predefined ${}^{e}\boldsymbol{z}_a, {}^{e}\boldsymbol{z}_{m,t}, {}^{s}\boldsymbol{A}_t, {}^{s}\boldsymbol{M}_t$, and quaternion multiplication, and finally can be denoted as follows:

$$\boldsymbol{\epsilon}({}^{s}_{e}\hat{\boldsymbol{q}}_t) = \begin{bmatrix} 2(\hat{q}_x\hat{q}_z - \hat{q}_0\hat{q}_y) - a_{x,t} \\ 2(\hat{q}_0\hat{q}_x + \hat{q}_y\hat{q}_z) - a_{y,t} \\ 2(0.5 - \hat{q}^2_x - \hat{q}^2_y) - a_{z,t} \\ 2\tilde{m}_x(0.5 - \hat{q}^2_y - \hat{q}^2_z) + 2\tilde{m}_y(\hat{q}_0\hat{q}_z + \hat{q}_x\hat{q}_y) + 2\tilde{m}_z(\hat{q}_x\hat{q}_z - \hat{q}_0\hat{q}_y) - m_{x,t} \\ 2\tilde{m}_x(\hat{q}_x\hat{q}_y - \hat{q}_0\hat{q}_z) + 2\tilde{m}_y(0.5 - \hat{q}^2_x - \hat{q}^2_z) + 2\tilde{m}_z(\hat{q}_0\hat{q}_x + \hat{q}_y\hat{q}_z) - m_{y,t} \\ 2\tilde{m}_x(\hat{q}_0\hat{q}_y + \hat{q}_x\hat{q}_z) + 2\tilde{m}_y(\hat{q}_y\hat{q}_z - \hat{q}_0\hat{q}_x) + 2\tilde{m}_z(0.5 - \hat{q}^2_x - \hat{q}^2_y) - m_{z,t} \end{bmatrix}.$$

Considering the natural presence of dynamic motion and magnetic disturbance conditions, as well as the inherent sensor errors, ρ_a and ρ_m are the weight factors for the acceleromter and megnetometer respectively. So the error objective function can be rewritten as $\boldsymbol{\epsilon}({}^{s}_{e}\hat{\boldsymbol{q}}_t) = [\rho_a\boldsymbol{\epsilon}_a\ \ \rho_m\boldsymbol{\epsilon}_m]^T$.

2) Fast Gauss–Newton Method: This section presents a new fast Gauss–Newton method that needs only one iteration calculation based on Literature [14]. According to the above-mentioned formulated problem, the conventional Gauss–Newton method consists of the following optimization steps:

$$\begin{aligned} {}^{s}_{e}\boldsymbol{q}(k+1) = {}^{s}_{e}\hat{\boldsymbol{q}}(k) - (\boldsymbol{J}(k)^T\boldsymbol{J}(k))^{-1}\boldsymbol{J}(k)^T\boldsymbol{\epsilon}({}^{s}_{e}\hat{\boldsymbol{q}}(k)) \\ (k = 0, 1, 2, \ldots, n) \end{aligned} \tag{12}$$

where k is an iteration number and $\boldsymbol{J}(k)$ is the Jacobian of $\boldsymbol{\epsilon}$, computed by using (13) at the bottom of the next page. K represents an constant 6×4 matrix consisting of ρ_a for the first three rows and ρ_m for the rest of rows, and the operator $.*$ represents matrix dot multiplication. Equation (12) describes the Gauss–Newton method for n iterations resulting in an orientation estimation of ${}^{s}_{e}\hat{\boldsymbol{q}}(n+1)$ based on an initial value ${}^{s}_{e}\hat{\boldsymbol{q}}(0)$. Actually, (12) can be rewritten as shown in

$$\begin{aligned} &{}^{s}_{e}\hat{\boldsymbol{q}}(n+1) \\ &= {}^{s}_{e}\hat{\boldsymbol{q}}(0) - \sum_{k=0}^{n}(\boldsymbol{J}(k)^T\boldsymbol{J}(k))^{-1}\boldsymbol{J}(k)^T\boldsymbol{\epsilon}({}^{s}_{e}\hat{\boldsymbol{q}}(k)) \\ &= {}^{s}_{e}\hat{\boldsymbol{q}}(0) - \lambda_k(\boldsymbol{J}(0)^T\boldsymbol{J}(0))^{-1}\boldsymbol{J}(0)^T\boldsymbol{\epsilon}({}^{s}_{e}\hat{\boldsymbol{q}}(0)). \end{aligned} \tag{14}$$

${}^{s}_{e}\hat{\boldsymbol{q}}(n+1)$ is actually the final optimal orientation at time $t+\Delta t$, denoted by ${}^{s}_{e}\hat{\boldsymbol{q}}_{a,t+\Delta t}$ (the subscript a indicates the orien-

tation estimated from the accelerometer and magnetometer) and ${}^s_e\hat{\boldsymbol{q}}(0)$ is the previous orientation estimation at time t, denoted by ${}^s_e\hat{\boldsymbol{q}}_{f,t}$ (the subscript f indicates the orientation estimation after complementary filter fusion). λ_k will change with every iteration to an optimal value. It is similar to the step-size in the GDA and is usually obtained based on the second derivative of the objective function, the Hessian. However, the GNA has the advantage that the second derivative, the Hessian, which can be challenging to compute, is not required, just approximated by $H \approx 2\boldsymbol{J}^T\boldsymbol{J}$ and finally combines the gradient $\boldsymbol{G} = 2\boldsymbol{J}^T\boldsymbol{\epsilon}$ together to obtain a much more efficient direction of gradient for convergence than the GDA, denoted by $\boldsymbol{\Delta} = -(\boldsymbol{J}^T\boldsymbol{J})^{-1}\boldsymbol{J}^T\boldsymbol{\epsilon}$. Even though the GNA requires less iterations than the GDA, it still increases the computing time. In fact, it is acceptable to compute one iteration per time period as long as the convergence rate governed by $\lambda_{t+\Delta t}$ shown in (15) is equal or greater than the physical rate of change of orientation. An appropriate value of $\lambda_{t+\Delta t}$, which guarantees the convergence rate of ${}^s_e\hat{\boldsymbol{q}}_{a,t+\Delta t}$, is restricted to the physical orientation rate measured from the gyroscope ${}^s_e\dot{\boldsymbol{q}}_{\omega,t+\Delta t}$ as this avoids overshooting due to an unnecessary large step size. Therefore, (14) can be simplified as (15) with only one iteration and an optimal value of $\lambda_{t+\Delta t}$ can be calculated as (16), which is defined the same as μ_t in [14]

$$\begin{aligned}
{}^s_e\hat{\boldsymbol{q}}_{a,t+\Delta t} &= {}^s_e\hat{\boldsymbol{q}}_{f,t} \\
&\quad - \lambda_{t+\Delta t}(\boldsymbol{J}({}^s_e\hat{\boldsymbol{q}}_{f,t})^T\boldsymbol{J}({}^s_e\hat{\boldsymbol{q}}_{f,t}))^{-1}\boldsymbol{J}({}^s_e\hat{\boldsymbol{q}}_{f,t})^T\boldsymbol{\epsilon}({}^s_e\hat{\boldsymbol{q}}_{f,t}) \\
&= {}^s_e\hat{\boldsymbol{q}}_{f,t} - \lambda_{t+\Delta t}\frac{\Delta\hat{\boldsymbol{q}}}{\|\Delta\hat{\boldsymbol{q}}\|} \qquad (15)\\
\lambda_{t+\Delta t} &= \alpha\|{}^s_e\dot{\boldsymbol{q}}_{\omega,t+\Delta t}\|\Delta t,\ \alpha > 1 \qquad (16)
\end{aligned}$$

where α is an augmentation of λ to account for noise in the accelerometer and magnetometer.

C. Adaptive-Gain Complementary Filter

As described in [29], a complementary filter is mainly designed for two noise sources with complementary spectral characteristics, so the idea is to pass the accelerometer and magnetometer signals through a low-pass filter and the gyroscope signals through a high-pass filter and combine them to give the final rate. Usually, the weight gain of the convention complementary filter for the measurement noise is a constant, while the proposed adaptive filter in this paper combines the advantage of the complementary filter and kalman filter, where time-variant parameters k_t and $(1-k_t)$ are set as the weights of each orientation for more robust results, denoted as (17). The gain k_t is adaptively adjusted by using the convergence rate $\lambda_t/\Delta t$ of low-frequency ${}^s_e\hat{\boldsymbol{q}}_{a,t}$ from vector observations based on the Gauss–Newton optimization method and the divergence rate β of high-frequency ${}^s_e\hat{\boldsymbol{q}}_{\omega,t}$ from the gyroscope, shown as group 3 in Fig. 3

$${}^s_e\hat{\boldsymbol{q}}_{f,t} = k_t{}^s_e\hat{\boldsymbol{q}}_{a,t} + (1-k_t){}^s_e\hat{\boldsymbol{q}}_{\omega,t},\ 0 \le k_t \le 1. \qquad (17)$$

Based on the same concept proposed in [14], the final orientation estimation can be obtained using

$$\begin{aligned}
{}^s_e\hat{\boldsymbol{q}}_{f,t+\Delta t} &= {}^s_e\hat{\boldsymbol{q}}_{f,t} + {}^s_e\dot{\boldsymbol{q}}_{f,t+\Delta t}\Delta t \\
{}^s_e\dot{\boldsymbol{q}}_{f,t+\Delta t} &= {}^s_e\dot{\boldsymbol{q}}_{\omega,t+\Delta t} - \beta{}^s_e\dot{\boldsymbol{q}}_{\epsilon,t+\Delta t} \\
{}^s_e\dot{\boldsymbol{q}}_{\epsilon,t+\Delta t} &= \frac{\Delta\hat{\boldsymbol{q}}}{\|\Delta\hat{\boldsymbol{q}}\|} \qquad (18)
\end{aligned}$$

where ${}^s_e\dot{\boldsymbol{q}}_{f,t+\Delta t}$ is the estimated orientation rate, which can be calculated as the rate of change of orientation measured by the gyroscope, ${}^s_e\dot{\boldsymbol{q}}_{\omega,t+\Delta t}$, with the magnitude of the gyroscope measurement error (usually zero-mean error), β, removed in the direction of the estimated error, $\dot{\boldsymbol{q}}_\epsilon$, computed from accelerometer and magnetometer measurements. β can be obtained using the method in [14].

D. Compensation Schemes

1) Gyroscope Bias Drift Compensation: With the disadvantage of accumulated drift over long-time tracking, ${}^s_e\dot{\boldsymbol{q}}_\epsilon$ is also used for the gyroscope bias drift compensation derived as the inverse to the relationship defined in (8). So the angular error ${}^s\boldsymbol{\omega}_e$, angular bias ${}^s\boldsymbol{\omega}_b$, and angular velocity ${}^s\boldsymbol{\omega}_c$ after compensation in each gyroscope axis can be expressed in (19) by using the normalized direction of $\dot{\boldsymbol{q}}_\epsilon$, shown as Group 2 in Fig. 3

$$\begin{aligned}
{}^s\boldsymbol{\omega}_{e,t+\Delta t} &= 2{}^s_e\hat{\boldsymbol{q}}^*_{f,t+\Delta t} \otimes {}^s_e\dot{\boldsymbol{q}}_{\epsilon,t+\Delta t} \\
{}^s\boldsymbol{\omega}_{b,t+\Delta t} &= \zeta\sum_{t+\Delta t}{}^s\boldsymbol{\omega}_{e,t+\Delta t}\Delta t \\
{}^s\boldsymbol{\omega}_{c,t+\Delta t} &= {}^s\boldsymbol{\omega}_{t+\Delta t} - {}^s\boldsymbol{\omega}_{b,t+\Delta t} \qquad (19)
\end{aligned}$$

where ζ accounts for the rate of convergence to remove nonzero-mean gyroscope measurement errors, which can be

$$\begin{aligned}
\boldsymbol{J}(k) = \frac{\partial\boldsymbol{\epsilon}}{\partial{}^s_e\hat{\boldsymbol{q}}(k)} &= \begin{bmatrix} \rho_a\frac{\partial\boldsymbol{\epsilon_a}}{\partial{}^s_e\hat{\boldsymbol{q}}(k)} \\ \rho_m\frac{\partial\boldsymbol{\epsilon_m}}{\partial{}^s_e\hat{\boldsymbol{q}}(k)} \end{bmatrix} = K.*\begin{bmatrix} \frac{\partial\boldsymbol{\epsilon_1}}{\partial\hat{q}_0} & \frac{\partial\boldsymbol{\epsilon_1}}{\partial\hat{q}_x} & \frac{\partial\boldsymbol{\epsilon_1}}{\partial\hat{q}_y} & \frac{\partial\boldsymbol{\epsilon_1}}{\partial\hat{q}_z} \\ \vdots & \vdots & \vdots & \vdots \\ \frac{\partial\boldsymbol{\epsilon_6}}{\partial\hat{q}_0} & \frac{\partial\boldsymbol{\epsilon_6}}{\partial\hat{q}_x} & \frac{\partial\boldsymbol{\epsilon_6}}{\partial\hat{q}_y} & \frac{\partial\boldsymbol{\epsilon_6}}{\partial\hat{q}_z} \end{bmatrix} \\
&= K.*\begin{bmatrix} -2\hat{q}_y & 2\hat{q}_z & -2\hat{q}_0 & 2\hat{q}_x \\ 2\hat{q}_x & 2\hat{q}_x & 2\hat{q}_z & 2\hat{q}_y \\ 0 & -4\hat{q}_x & -4\hat{q}_y & 0 \\ 2\tilde{m}_y\hat{q}_z - 2\tilde{m}_z\hat{q}_y & 2\tilde{m}_y\hat{q}_y + 2\tilde{m}_z\hat{q}_z & -4\tilde{m}_x\hat{q}_y + 2\tilde{m}_y\hat{q}_x - 2\tilde{m}_z\hat{q}_0 & -4\tilde{m}_x\hat{q}_z + 2\tilde{m}_y\hat{q}_0 + 2\tilde{m}_z\hat{q}_x \\ -2\tilde{m}_x\hat{q}_z + 2\tilde{m}_z\hat{q}_x & 2\tilde{m}_x\hat{q}_y - 4\tilde{m}_y\hat{q}_x + 2\tilde{m}_z\hat{q}_0 & 2\tilde{m}_x\hat{q}_x + 2\tilde{m}_z\hat{q}_z & -2\tilde{m}_x\hat{q}_0 - 4\tilde{m}_y\hat{q}_z + 2\tilde{m}_z\hat{q}_y \\ 2\tilde{m}_x\hat{q}_y - 2\tilde{m}_y\hat{q}_x & 2\tilde{m}_x\hat{q}_z - 2\tilde{m}_y\hat{q}_0 - 4\tilde{m}_z\hat{q}_x & 2\tilde{m}_x\hat{q}_0 + 2\tilde{m}_y\hat{q}_z - 4\tilde{m}_z\hat{q}_y & 2\tilde{m}_x\hat{q}_x + 2\tilde{m}_y\hat{q}_y \end{bmatrix} \qquad (13)
\end{aligned}$$

similarly determined as β by using numerical experimental data.

2) Accelerometer and Magnetometer Compensation: In order to select the best reliable vectors among the sensor measurements as inputs to the filter, accelerometer and magnetometer measurements should be compensated. For example, ${}^{s}\boldsymbol{A}_t$ during fast motion conditions and ${}^{s}\boldsymbol{M}_t$ under temporary magnetic disturbances cannot be totally trusted as reliable information. Therefore, under these conditions, ${}^{s}\boldsymbol{\omega}$ is more trustful measurement information.

Following the aforementioned concept, the input vectors ${}^{s}\boldsymbol{A}$ (gravity-related) and ${}^{s}\boldsymbol{M}$ (magnetic field-related) for the Gauss–Newton optimization algorithm can be compensated [see Group 1.1 in Fig. 3] using three steps: 1) The reference vector ${}^{e}\boldsymbol{z}_m$ for the earth's magnetic field at time t will be adaptively changed [see Group 1.2 in Fig. 3], where we didn't use the method in [14]. This method has a disadvantage of angle drift at $t = 0$, because the author normalized the measured direction of the earth's magnetic field to have only components in the earth frame x and z axes and ignored the components in the earth frame y axis (see details in [14]); 2) They are conditionally selected using reference vectors ${}^{e}\boldsymbol{z}_a$ or ${}^{e}\boldsymbol{z}_{m,t}$; and 3) The filter gain is adaptively adjusted as mentioned in Section IV-C to compensate for not only the aforesaid conditions but also the accumulated gyro-integrated orientation error. In order to detect perturbed situations online, the following criteria, which are similarly used in [23], but more robust with the adaptive reference vector selection for earth's magnetic field, are implemented in this paper

$$
{}^{s}\boldsymbol{A}_t = \begin{cases} \frac{{}^{s}\boldsymbol{a}_t^m}{\|{}^{s}\boldsymbol{a}_t^m\|}, & \text{if } |\|{}^{s}\boldsymbol{a}_t^m\| - \|\boldsymbol{g}\|| \le \varepsilon_a \\ {}^{s}_{e}\hat{\boldsymbol{q}}^{*}_{t-\Delta t} \otimes {}^{e}\boldsymbol{z}_a \otimes {}^{s}_{e}\hat{\boldsymbol{q}}_{t-\Delta t}, & \text{otherwise} \end{cases}
$$

$$
{}^{e}\boldsymbol{z}_{m,t} = \begin{cases} \frac{{}^{s}\boldsymbol{m}_{t=0}^m}{\|{}^{s}\boldsymbol{m}_{t=0}^m\|}, & \text{if } |\|{}^{s}\boldsymbol{m}_t^m\| - \|\boldsymbol{m}_{t=0}\|| \le \varepsilon_m \\ {}^{s}_{e}\hat{\boldsymbol{q}}_{t-\Delta t} \otimes {}^{s}\boldsymbol{M}_{t-\Delta t} \otimes {}^{s}_{e}\hat{\boldsymbol{q}}^{*}_{t-\Delta t}, & \text{otherwise} \end{cases}
$$

$$
{}^{s}\boldsymbol{M}_t = \begin{cases} \frac{{}^{s}\boldsymbol{m}_t^m}{\|{}^{s}\boldsymbol{m}_t^m\|}, & \text{if } |\|{}^{s}\boldsymbol{m}_t^m\| - \|\boldsymbol{m}_{t=0}\|| \le \varepsilon_m \\ {}^{s}_{e}\hat{\boldsymbol{q}}^{*}_{t} \otimes {}^{e}\boldsymbol{z}_{m,t} \otimes {}^{s}_{e}\hat{\boldsymbol{q}}_{t}, & \text{otherwise} \end{cases}.
$$

E. Filter Gains

In this paper, two filter gains β and ζ should be determined. The filter gain β accounts for all zero-mean gyroscope measurement errors, expressed as the magnitude of a quaternion derivation. These errors usually come from sensor noise, signal aliasing, quantization errors, calibration errors, sensor missalignment, sensor axes nonorthogonality, and frequency response characteristics. The filter gain ζ denotes the rate of convergence to especially remove nonzero-mean gyroscope measurement errors, also expressed as the magnitude of a quaternion derivative. Both of these errors represent the gyroscope bias. In order to define β and ζ, $\tilde{\boldsymbol{\omega}}_\beta$ and $\tilde{\dot{\boldsymbol{\omega}}}_\zeta$ are used, where $\tilde{\boldsymbol{\omega}}_\beta$ denotes the estimated mean zero gyroscope measurement error for three axes x, y and z, and $\tilde{\dot{\boldsymbol{\omega}}}_\zeta$ denotes the estimated rate of gyroscope bias drift for three axes x, y and z. $\tilde{\boldsymbol{\omega}}_\beta$ and $\tilde{\dot{\boldsymbol{\omega}}}_\zeta$ can be easily determined by numerical experiments. Based on the relationship described by (8), β, and ζ can be defined by (20) and (21), respectively, where $\hat{\boldsymbol{q}}$ is any unit quaternion

$$
\beta = \|\frac{1}{2}\hat{\boldsymbol{q}} \otimes [0\ \tilde{\boldsymbol{\omega}}_\beta]\| = \sqrt{\frac{3}{4}}\|\tilde{\boldsymbol{\omega}}_\beta\| \tag{20}
$$

$$
\zeta = \|\frac{1}{2}\hat{\boldsymbol{q}} \otimes [0\ \tilde{\dot{\boldsymbol{\omega}}}_\zeta]\| = \sqrt{\frac{3}{4}}\|\tilde{\dot{\boldsymbol{\omega}}}_\zeta\|. \tag{21}
$$

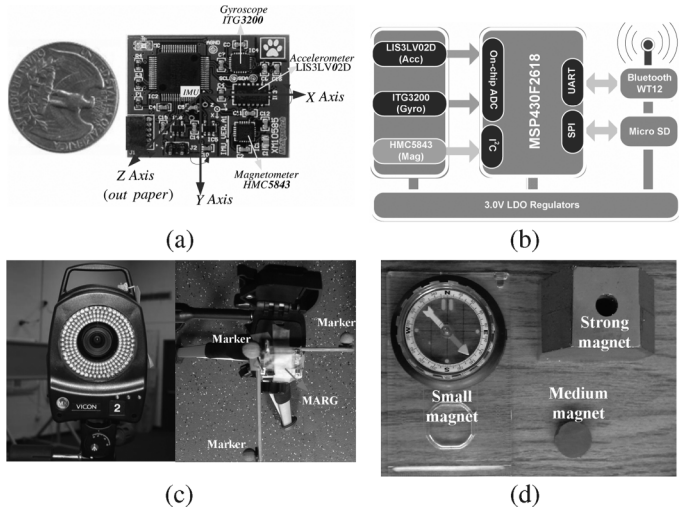

Fig. 4. Prototype and Hardware design for MARG sensor arrays and experimental illustrations. (a) The top view and its frame. (b) Block diagram. (c) Illustration of Test II and III. (d) Illustration of Test I.

V. Experimental Validation and Results

A. Experimental Validation

To verify the proposed algorithm, which is implemented in C++, a MARG platform is developed. Fig. 4(a) shows the newly developed MARG sensor, which contains a tri-axis gyroscope (ITG3200), a tri-axis accelerometer (LIS3LV02D), and a tri-axis magnetometer (HMC5843) in a small sensor package measuring rotational body kinematics without the need for an external reference. The small chip also has an embedded processor (TI MSP430F2618) for computation. The block diagram of the wearable sensor node is shown in Fig. 4(b). All sensor signals were sampled at 40 *Hz* and interfaced to a PC via Bluetooth, which are convenient for human motion tracking and analysis.

In order to verify the orientation estimation accuracy, the root mean square (rms) error value of Euler angles (roll, pitch, and yaw) from the quaternion-based orientation is chosen as the criterion to evaluate the static and dynamic performance of the proposed AGOF method. A Vicon system [12] shown in Fig. 4(c) was used to provide reference measurement for testing the dynamic accuracy of the proposed method. For the static accuracy, three other well-known algorithms were used to compare with the proposed AGOF within magnetic distortion, which include the Kalman-based filter (KF), factored quaternion algorithm (FQA) proposed by [13], and gradient descent algorithm (GDA) proposed by [14]. The magnetic distortion can be generated by swaying a magnetic iron, shown in Fig. 4(d). Ac-

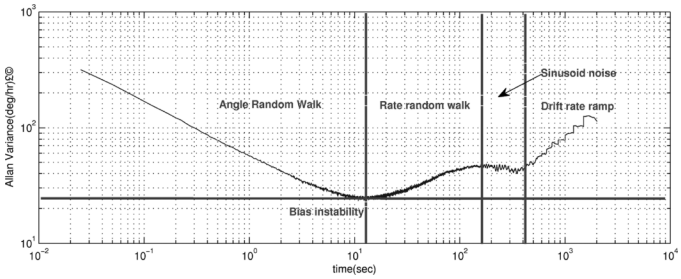

Fig. 5. Allan-variance analysis chart for our low-cost gyroscope.

tually, the author in [14] only presented the results for introducing bias to x-axis and y-axis of the gyroscope. However, his method cannot work well for introducing bias to z-axis of the gyroscope, which severely affects the yaw angle estimate. Therefore, neither works well for the low-cost gyroscope with time-varying bias. Fig. 5 shows an Allan-variance analysis chart for a sample of the gyroscope embedded in the newly developed MARG sensor, which indicates a high level of bias instability. Considering that the proposed method has advantages of the Gauss–Newton optimizer and adaptive measurement vectors selection, it is more robust to handle this problem. The weight factor in the GNA, filter gains for the complementary filter, and the threshold values in the vector selections were set as $\rho_a = 1$, $\rho_m = 1$, $\beta = 0.0756$, $\zeta = 0.003$, $\varepsilon_a = 0.25\ \mathrm{m/s^2}$, and $\varepsilon_m = 0.02$ Guass.

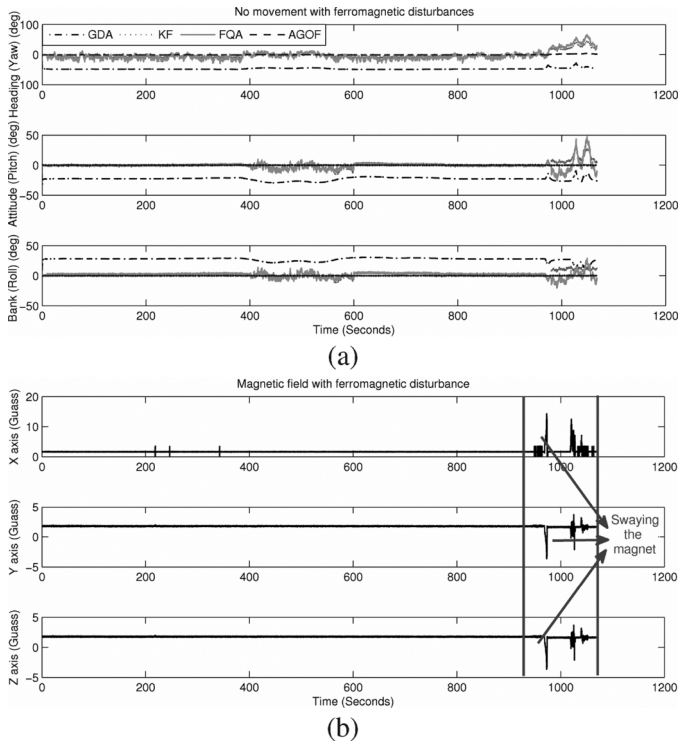

Fig. 6. Static orientation estimation with magnetic disturbances using the proposed AGOF with vector selections compared with the GDA, KF, and FQA. (a) Static orientation estimation with magnetic disturbances. (b) Distorted magnetic field.

B. Experimental Results

1) Test I: No Movement With Magnetic Disturbances: In this test scenario, the sensor arrays kept still and a magnetic shown in Fig. 4(d) was swayed around the sensor intermittently. The magnetic disturbances for three axes were clearly shown in Fig. 6(b), marked in the red area. Fig. 6(a) shows the Euler angles which were calculated from the GDA, KF, FQA, and AGOF. It is obvious that all Euler angles were affected by the magnetic disturbances using the GDA, KF, and FQA, while there was no obvious affection for any of them based on the proposed AGOF with the adaptive vector sections.

2) Test II: Slow Movement Within a Magnetically Homogeneous Environment: During this test, the MARG sensor moved within a magnetically homogeneous environment which had no significant ferromagnetic disturbances, and also the accelerometer rarely experienced extra accelerations. This test involved three typical motions (single roll, pitch and yaw movements) and the results from the Vicon system were used as the ground truth to test the accuracy of the proposed method. Fig. 7 shows the measured and estimated angles in upper plot and estimated errors in lower plot. It is clearly seen that estimated errors for the roll, pitch, and yaw were very small and the rms error was used to quantificationally describe them.

3) Test III: Sudden Fast Movement Within a Magnetically Homogeneous Environment: Test III was performed in a magnetically homogeneous environment but the MARG sensor went through a sudden acceleration change [see Fig. 8(b) in red area]. As shown in Fig. 8(a), the proposed AGOF offered reasonably accurate estimation performance even in this situation, compared with the measured results from the Vicon. However, using the GDA , KF, and FQA, the corresponding estimated angles were far from the actual values and had obvious drifts after returning to the initial state.

4) Gyroscope Bias Drift Estimation With Magnetic Disturbances for Test I: Actually, the calibrated gyroscope data used in [14] did not contain any bias errors. However, the newly developed chip still has bias even after calibration. Therefore, a gyroscope bias drift compensation algorithm was developed in this paper. Fig. 9(a) shows the estimated results of the gyroscope x, y, and z axis biases using the proposed AGOF and the GDA proposed by Madgwick within magnetic disturbances, plotted against the actual gyroscope measurements. From these results, the proposed AGOF can be seen to successfully estimate the gyroscope biases even within magnetic disturbances, while Madgwick's method presented wrong estimation.

5) Static and Dynamic Accuracy: The static and dynamic rms error values of Euler angles were calculated based on Test I, II, and III to test the accuracy of the proposed AGOF, KF, GNA, and FQA. For the static accuracy, it was evaluated with and without magnetic distortion. Table I shows three Euler angles' rms errors of static and dynamic movements from four methods. From these data, it can be clearly seen that the proposed AGOF is more accurate than all other three methods. Moreover, the proposed AGOF can achieve not only real-time tracking but also

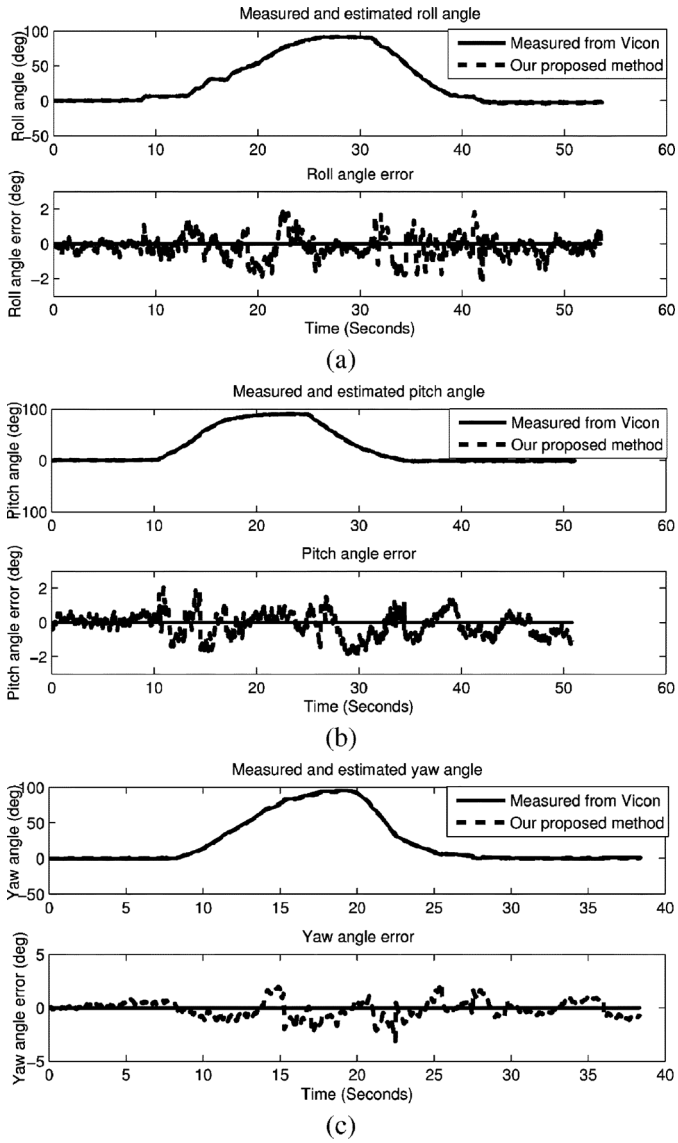

Fig. 7. Typical results for each measured and estimated angle (top) and error (bottom). (a) Roll angle and error. (b) Pitch angle and error. (c) Yaw angle and error.

high accuracy, which is less than 2°, even when there are significant ferromagnetic disturbances and fast dynamic movements.

6) Real-Time Orientation Visualization: Fig. 10 shows a 3-D coordinate system (Red-X axis, Green-Y axis and Blue-Z axis) demonstration of real-time orientation tracking estimated by the newly developed MARG sensor. The 3-D visualization is illustrated on the user PC by using the OpenGL. First, an initial position is depicted in Fig. 10(a), and then rotating results around X, Y and Z axis are shown in Fig. 10(b), (c), and (e), respectively. Fig. 10(f) demonstrates the high accuracy of the proposed method even with strong magnetic distortion.

7) Motion Capture of Human Upper Limb: The upper limb of human body can be modeled as a skeleton structure that has two segments linked by three joints (shoulder, elbow, and wrist), and two MARG sensors are used to attach two segments, respectively. Fig. 11 shows the real pose of the upper limb and the visualization of its estimation by MARG sensors. Supposing the origin of the coordinate is located at the shoulder, the posture of upper limb can be tracked in real-time using the proposed method in this paper to estimate the orientation of these two sensor nodes.

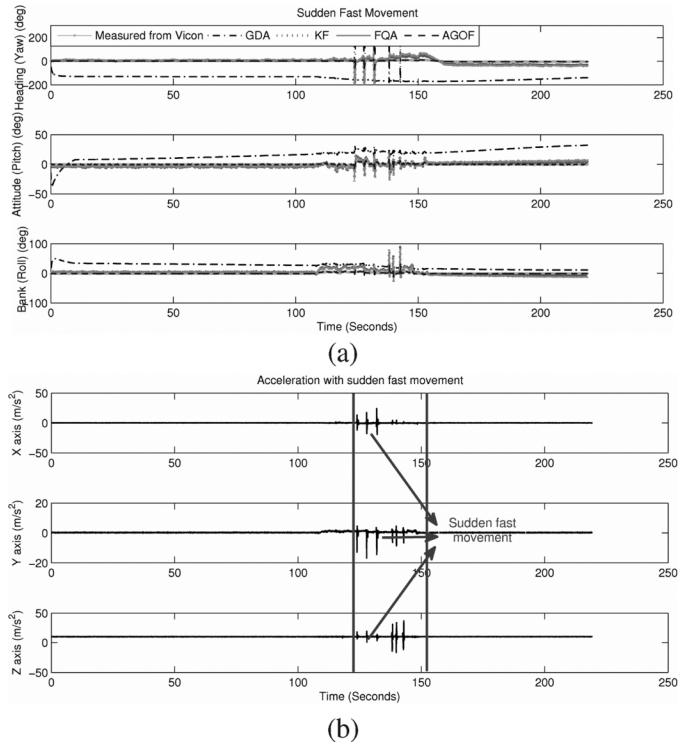

Fig. 8. Orientation estimation with sudden fast movement using the proposed AGOF with vector selections compared with the GDA, KF, and FQA. (a) Orientation estimation with sudden fast movement. (b) Acceleration data.

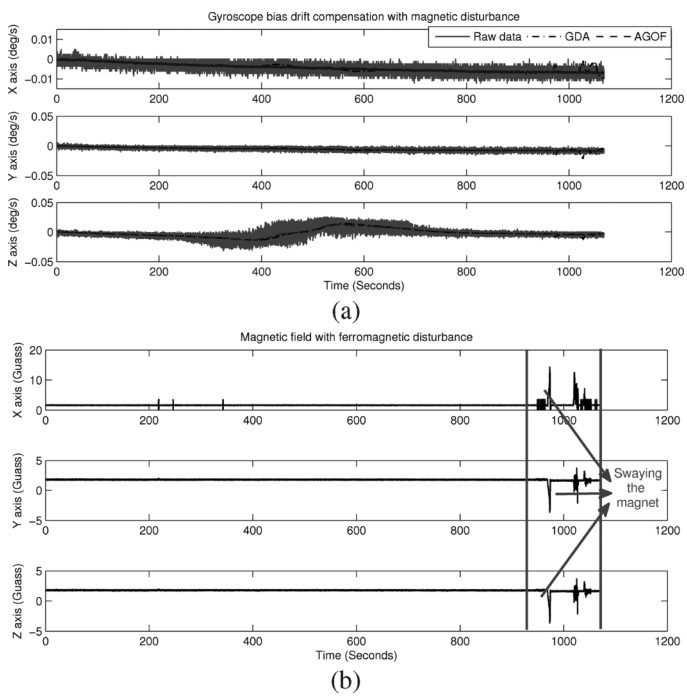

Fig. 9. Gyroscope bias drift estimation for each axis using the AGOF compared with the GDA. (a) Gyroscope bias drift estimation for each axis. (b) Distorted magnetic field.

TABLE I
STATIC AND DYNAMIC ACCURACY OF METHODS FROM THE AGOF, KF, GDA AND FQA (MD:MAGNETIC DISTORTION)

Euler angles \ Methods	AGOF	KF	GDA	FQA
RMS[Roll] Static without MD :	0.2316°	0.7890°	0.5811°	1.2311°
RMS[Roll] Static with MD:	0.2910°	8.2316°	9.1831°	9.4256°
RMS[Roll] Dynamic:	0.6645°	3.8695°	2.8252°	12.5791°
RMS[Pitch] Static without MD :	0.2664°	0.8191°	0.5023°	1.3813°
RMS[Pitch] Static with MD:	0.2742°	8.5142°	9.2472°	9.0811°
RMS[Pitch] Dynamic:	0.6018°	3.3471°	2.6680°	13.2781°
RMS[Yaw] Static without MD :	0.5322°	1.1572°	1.0734°	1.5193°
RMS[Yaw] Static with MD:	0.9496°	11.1532°	10.5811°	20.8124°
RMS[Yaw] Dynamic:	0.8182°	8.5451°	10.1101°	15.1125°
Real-time Tracking	Yes	No	Yes	No
Gyro Drift Compensation	Yes	No	Yes	No
MD Compensation	Yes	No	Yes	No
Accelerometer Compensation	Yes	No	No	No

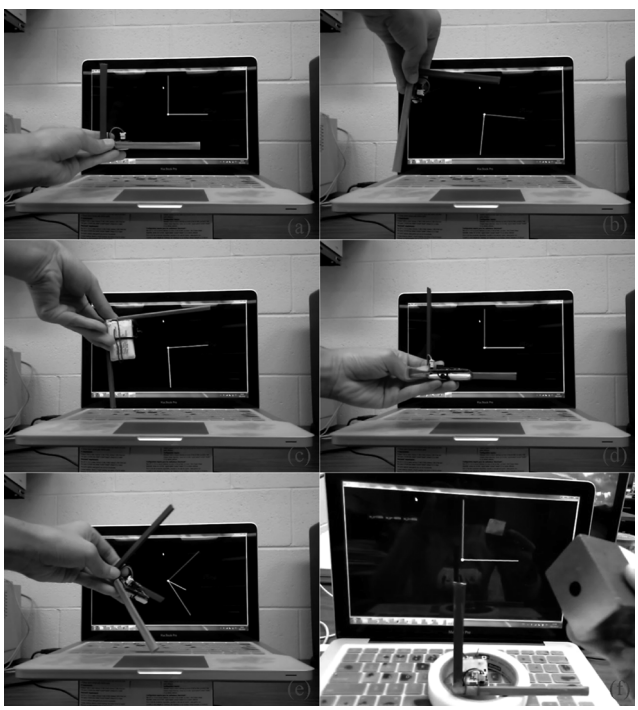

Fig. 10. Real-time 3-D orientation visualization of MARG sensor: (a) initial position; (b) rotating around Y axis; (c) rotating around X axis; (d) rotating around Z axis; (e) Random rotating around X, Y and Z axis together; (f) static demonstration with strong magnetic distortion.

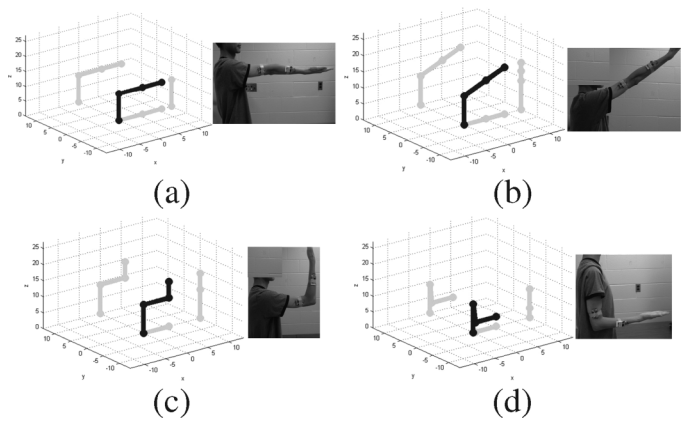

Fig. 11. Motion capture of human upper limb. On the right side of each photograph: a user wearing the MARG sensors is moving his upper limb. On the left side: the real-time reconstruction of the movements and shadows of human upper limb in each plane. (a) Initial position. (b) Rotation I. (c) Rotation II. (d) Rotation III.

VI. CONCLUSION

This paper presented an AGOF with adaptive vector selections designed for real-time human motion tracking in free-living environments. This paper focused on alleviating the computational load, accumulated sensing errors, and developed a simple and fast algorithm using an adaptive-gain complementary filter based on the fast convergence rate from the Gauss–Newton optimization algorithm and the divergence rate from the gyroscope. In particular, the proposed method is effective at handling severe magnetic distortion and high dynamic movement with the compensation schemes for each sensor. The rms error of the estimated orientation is less than two degrees, which can be compared with current proprietary commercial algorithms. Due to its high computational efficiency and accuracy, the proposed algorithm can be potentially implemented in a network of miniature MARG sensors for human body movement, forming a truly portable and ambulatory motion tracking system. This paper demonstrated the human-upper-limb-motion-capture using the proposed method, and the results also illustrated the high accuracy.

Due to the performance, size, and weight of MARG sensors, they could easily be further embedded in a track suit for total body motion construction. Therefore, it could be used as a surveillance system in patients' home environments for therapists to monitor patients' behavior. Thus, it might lead to optimal solutions for therapy efficiency and expense issues, especially given the increasing demand for health-care services and increasing expense in national health service.

REFERENCES

[1] H. Zhou and H. Hu, "Human motion tracking for rehabilitation—A survey," *Biomed. Signal Process. Control*, vol. 3, no. 1, pp. 1–18, 2008.

[2] S. Patel, R. Hughes, T. Hester, J. Stein, M. Akay, J. Dy, and P. Bonato, "A novel approach to monitor rehabilitation outcomes in stroke survivors using wearable technology," *Proc. IEEE*, vol. 98, no. 3, pp. 450–461, Mar. 2010.

[3] U. Laessoe, H. C. Hoeck, O. Simonsen, T. Sinkjaer, and M. Voigt, "Fall risk in an active elderly population—Can it be assessed?," *J. Negative Results BioMed.*, vol. 6, no. 2, p. 2, 2007.

[4] A. G. Cutti, A. Giovanardi, L. Rocchi, A. Davalli, and R. Sacchetti, "Ambulatory measurement of shoulder and elbow kinematics through inertial and magnetic sensors," *Med. Biol. Eng. Comput.*, vol. 46, no. 2, pp. 169–178, 2008.

[5] K. D. Nguyen, I. M. Chen, Z. Luo, S. H. Yeo, and H. B. L. Duh, "A body sensor network for tracking and monitoring of functional arm motion," in *Proc. IEEE/RSJ Int. Conf. Intell. Robots Syst.*, 2009, pp. 3862–3867.

[6] K. D. Nguyen, I. M. Chen, Z. Luo, S. H. Yeo, and H. B. L. Duh, "A wearable sensing system for tracking and monitoring of functional arm movement," *IEEE/ASME Trans. Mechatron.*, vol. 16, no. 2, pp. 213–220, 2011.

[7] M. M. B. Morrow, K. R. Kaufman, and K. N. An, "Shoulder model validation and joint contact forces during wheelchair activities," *J. Biomechan.*, vol. 43, no. 13, pp. 2487–2492, 2010.

[8] H. Zhou, H. Hu, and N. Harris, "Wearable inertial sensors for arm motion tracking in home-based rehabilitation," in *Proc. 9th Int. Conf. Intell. Automous Syst.*, 2006, pp. 930–937.

[9] X. Yun, M. Lizarraga, E. R. Bachmann, and R. B. McGhee, "An improved quaternion-based Kalman filter for real-time tracking of rigid body orientation," in *Proc. IEEE/RSJ Int. Conf. Intell. Robots Syst.*, 2003, vol. 2, pp. 1074–1079.

[10] F. Mohd-Yasin, D. J. Nagel, and C. E. Korman, "Noise in MEMS," *Measurement Sci. Technol.*, vol. 21, no. 1, p. 012001, 2010.

[11] E. R. Bachmann, X. Yun, and A. Brumfield, "Limitations of attitude estimation algorithms for inertial/magnetic sensor modules," *IEEE Robot. Automat. Mag.*, vol. 14, no. 3, pp. 76–87, Sep. 2007.

[12] Vicon Motion Capture Systems [Online]. Available: http://www.vicon.com

[13] X. Yun, E. R. Bachmann, and R. B. McGhee, "A simplified quaternion-based algorithm for orientation estimation from earth gravity and magnetic field measurements," *IEEE Trans. Instrum. Meas.*, vol. 57, no. 3, pp. 638–650, Mar. 2008.

[14] S. O. H. Madgwick, A. J. L. Harrison, and R. Vaidyanathan, "Estimation of IMU and MARG orientation using a gradient descent algorithm," in *Proc. IEEE Int. Conf. Rehabil. Robot.*, 2011, vol. 51, pp. 1–7.

[15] H. J. Luinge and P. H. Veltink, "Measuring orientation of human body segments using miniature gyroscopes and accelerometers," *Med. Biol. Eng. Comput.*, vol. 43, no. 2, pp. 273–282, 2005.

[16] H. J. Luinge, P. H. Veltink, and C. T. M. Baten, "Estimating of orientation with gyroscopes and accelerometers (student paper finalist)," in *Proc. 1st Joint BMES/EMBS Conf. Serving Humanity, Advancing Technol.*, 1999, vol. 2, p. 844.

[17] T. Harada, H. Uchino, T. Mori, T. Sato, and B. K. Hongo, "Portable absolute orientation estimation device with wireless network under accelerated situation," in *Proc. IEEE Int. Conf. Robot. Automat.*, 2004, vol. 2, pp. 1412–1417.

[18] A. M. Sabatini, "Quaternion-based extended Kalman filter for determining orientation by inertial and magnetic sensing," *IEEE Trans. Biomed. Eng.*, vol. 53, no. 7, pp. 1346–1356, Jul. 2006.

[19] D. Roetenberg, H. J. Luinge, C. T. M. Baten, and P. H. Veltink, "Compensation of magnetic disturbances improves inertial and magnetic sensing of human body segment orientation," *IEEE Trans. Neural Syst. Rehabil. Eng.*, vol. 13, no. 3, pp. 395–405, Sep. 2005.

[20] G. Welch and G. Bishop, *An Introduction to the Kalman Filter*. Chapel Hill: Univ. North Carolina, 1995.

[21] G. Wahba, "A least squares estimate of spacecraft attitude," *SIAM Rev.*, vol. 7, no. 3, p. 409, 1965.

[22] M. D. Shuster and S. D. Oh, "Three-axis attitude determination from vector observations," *J. Guidance Control Dynam.*, vol. 4, no. 1, pp. 70–77, 1981.

[23] J. K. Lee and E. J. Park, "A fast quaternion-based orientation optimizer via virtual rotation for human motion tracking," *IEEE Trans. Biomed. Eng.*, vol. 56, no. 5, pp. 1574–1582, May 2009.

[24] R. Mahony, T. Hamel, and J. Pflimlin, "Nonlinear complementary filters on the special orthogonal group," *IEEE Trans. Automatic Control*, vol. 53, no. 5, pp. 1203–1218, Jun. 2008.

[25] M. Euston, P. Coote, R. Mahony, J. Kim, and T. Hamel, "A complementary filter for attitude estimation of a fixed-wing UAV," in *Proc. IEEE/RSJ Int. Conf. Intell. Robots Syst.*, 2008, pp. 340–345.

[26] J. Calusdian, X. Yun, and E. Bachmann, "Adaptive-gain complementary filter of inertial and magnetic data for orientation estimation," in *Proc. IEEE/RSJ Int. Conf. Robot. Automat. (ICRA)*, 2011, pp. 1916–1922.

[27] J. C. K. Chou, "Quaternion kinematic and dynamic differential equations," *IEEE Trans. Robot. Automat.*, vol. 8, no. 1, pp. 53–64, Feb. 1992.

[28] B. K. P. Horn, "Closed-form solution of absolute orientation using unit quaternions," *J. Opt. Soc. Am. A*, vol. 4, no. 4, p. 629, 1987.

[29] E. R. Bachmann, "Inertial and magnetic tracking of limb segment orientation for inserting humans into synthetic environments," Ph.D. dissertation, Naval Postgraduate School, Monterey, CA, 2000.

Ya Tian (S'12) was awarded a scholarship under the State Scholarship Fund to pursue her Ph.D. study in electrical engineering at Michigan Technological University, Houghton, in 2009, and received the Ph.D. degree in 2012. She is currently an Assistant Professor in the School of Information and Electrical Engineering, Shandong Jianzhu University, Jinan, Shandong, China. She mainly aims at human motion tracking and rehabilitation with wearable sensors, and blind navigation.

Hongxing Wei (M'12) received the Ph.D. degree from the College of Automation, Harbin Engineering University, Harbin, China, in 2001.

He is currently an Associate Professor in the School of Mechanical Engineering and Automation, Beihang University, Beijing, China. His research interests include self-assembly swarm robots, modular robotics architecture, mobile sensor networks, and embedded systems.

Jindong Tan (M'02) received the Ph.D. degree in electrical and computer engineering from Michigan State University, East Lansing, in 2002.

He is currently an Associate Professor in Department of Mechanical, Aerospace and Biomedical Engineering, The University of Tennessee, Knoxville. He has been an Assistant/Associate Professor in the Department of Electrical and Computer Engineering at Michigan Technological University, Houghton. His research interests include mobile sensor networks, augmented reality and biomedical imaging, dietary assessment, and mobile manipulation.

Dr. Tan is a member of the ACM and Sigma Xi.